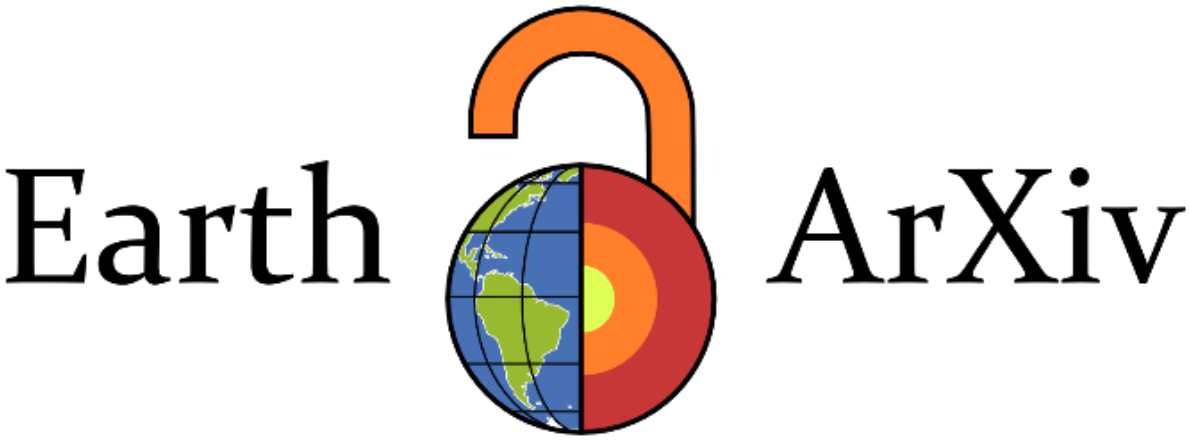

Climate mitigation benefits emerge within a decade

Assaf Shmuel[1,*], Niklas Schwind[1,2], Kai Kornhuber[1,3], Ron Milo[4],

Carl-Friedrich Schleussner[1,5]

[1] International Institute for Applied Systems Analysis (IIASA), Laxenburg, Austria

[2] Geography Department, Humboldt University of Berlin, Berlin, Germany

[3] Lamont Doherty Earth Observatory, Columbia University, NYC, New York, USA

[4] Department of Plant and Environmental Sciences, Weizmann Institute of Science, 76100 Rehovot, Israel

[5] Integrative Research Institute on Transformations of Human-Environment Systems (IRI THESys) and the Geography Department, Humboldt-Universität zu Berlin, Berlin, Germany

* Corresponding author: shmuel@iiasa.ac.at

Abstract

Discernible differences in global climate responses under varying greenhouse gas emission scenarios are commonly assumed to emerge only after 20 to 30 years. Here we show that mitigation benefits are detectable within a decade (9±6 years) over the global land area when high-resolution gridded climate data are analysed with a machine learning approach. By retaining spatial information, we uncover regional warming signals that remain hidden when relying on global averages and identify the regions in which these signals first emerge using an explainability framework. Even when restricting our analysis to subregions, we find a detectable signal to emerge over the land area of the four highest emitting countries in 13 (±6) years. These results demonstrate that detectable climate benefits of greenhouse gas mitigation appear much earlier than previously recognised and suggest that high emitting countries would also experience near-term benefits from bending the emissions curve.

Introduction

Earth's climate is undergoing rapid and unprecedented changes due to human activities, primarily driven by the burning of fossil fuels (1, 2). The consequences of climate change are already being felt worldwide, including rising global

temperatures, more frequent and intense extreme weather events (3, 4), prolonged droughts (5), and elevated wildfire risks (6). These impacts are expected to worsen in the coming decades, with profound consequences for ecosystems, economies, and human well-being (7–9).

Stringent mitigation efforts by reducing greenhouse gas emissions towards achieving global net-zero are essential to limiting future warming and minimizing climate-related risks. However, current mitigation efforts remain insufficient, and global emissions have not yet peaked, let alone begun the rapid decline required to meet the goals of the Paris Agreement (10).

Assessing the emergence of tangible climate benefits of emission reductions is central in the context of the political and private sector incentives to increase the commitment for climate action. This timing is policy-relevant because detectable near-term benefits help sustain support for ambitious emissions reductions (11, 12). In its Sixth Assessment Report, the Intergovernmental Panel on Climate Change (IPCC) reports that discernible differences in global surface temperature between scenarios emerge within around 20 years (13). Here, emergence time is defined as the point at which the forced response becomes distinguishable from internal climate variability with statistical confidence. On shorter time-scales, the effect of changes in short-lived climate forcers including natural climate variability and aerosols may obscure the imprint of greenhouse gas mitigation (14–16), at least when focusing on single time series such as global averaged climate indicators (11). Previous studies have shown that the temperature response from emissions peaks after about a decade, suggesting a short response timescale that could be masked by internal climate variability (17). The question of the detectability of tangible mitigation benefits is ultimately one of ensemble size, target variable of interest, and methodological approach. Using very large-ensemble simulations based on climate model emulation, ref. (18) found that stringent emission reductions in the near-term could halve the rate of warming over a 20 year period compared to a current policy pathway.

Methods based on classical statistics can be limited in terms of the information they consider and often require assumptions on statistical relationships. Furthermore, they often focus on time series, for example regionally, or globally aggregated

information (14–16). This means that they do not take full advantage of all available spatial information, implying that important regional or local features such as differences in the pace of climate change depending on latitude or altitude, as well as differences in natural variability, may be missed (19).

In this study, we introduce a machine learning (ML) approach to assess regional and global near surface temperature responses under intermediate and low emissions scenarios. Unlike traditional approaches, our ML model can uncover complex patterns in climate data to assess subtle but consistent signals of mitigation (20–23). This approach aligns with recent work highlighting the growing role of explainable artificial intelligence in the geosciences and climate research (24–27). By training ML models on large-scale climate simulations, we can determine the earliest point in time at which mitigation effects become distinguishable from unmitigated climate trajectories, focusing on monthly temperature at grid cell level. Additionally, by applying explainability techniques, we pinpoint the regions with early emergence, providing insight into where mitigation efforts yield the most immediate discernible benefits (24, 28).

Results

We apply a gradient boosting decision tree classifier (LightGBM (29)) to detect differences between emissions scenarios, focusing on the comparison between spatial and temporal patterns in gridded land temperature data (excluding Greenland and Antarctica) of low- and intermediate-emissions pathways (SSP1-2.6 and SSP2-4.5 respectively). The model is trained on monthly near-surface air temperature fields from CMIP6 ensembles, remapped to a 2.5° × 2.5° land grid (30). This method aims to separate the long-term warming signal from natural variability, thus unmasking earliest emergence times. For context, we compare these results with a baseline model that relies only on the global mean temperature. Further experimental details are provided in the Methods section.

Detection of mitigation benefits within a decade

Differences in the global climate response to a low and intermediate emission scenario can be detected within a decade (Fig. 1). This contrasts with earlier estimates, which place the time-of-emergence at 20–30 years (13–15). The

year-by-year performance of the model is shown in Fig. 1 (panel A, blue curve). Model performance is quantified using the ROC AUC (area under the receiver operating characteristic curve), a standard classification metric (31, 32). A ROC AUC score of 1 indicates perfect classification performance, whereas a score of 0.5 suggests the model's predictions are no better than random (31).

Within 9±6 years the model's mean predictive skill and its one standard deviation confidence interval both rise above 0.5, indicating a statistically meaningful improvement in distinguishing between the low- and intermediate-emissions scenarios, while in the initial years (years 0-5), the predictive skill of the full model is close to random guessing (AUC=0.5) because differential long-term warming trends have not yet emerged from among the natural variability. By comparison, a baseline logistic regression model that uses only global mean surface air temperature (orange curve) shows a statistically significant departure from random guessing only after ≈30 years. The differences in emissions and global mean temperature (GMT) between the two scenarios are shown in Fig. 1B. GMT differences between the two scenarios remain indistinguishable for ≈30 years from the start, in line with previous studies (14, 16).

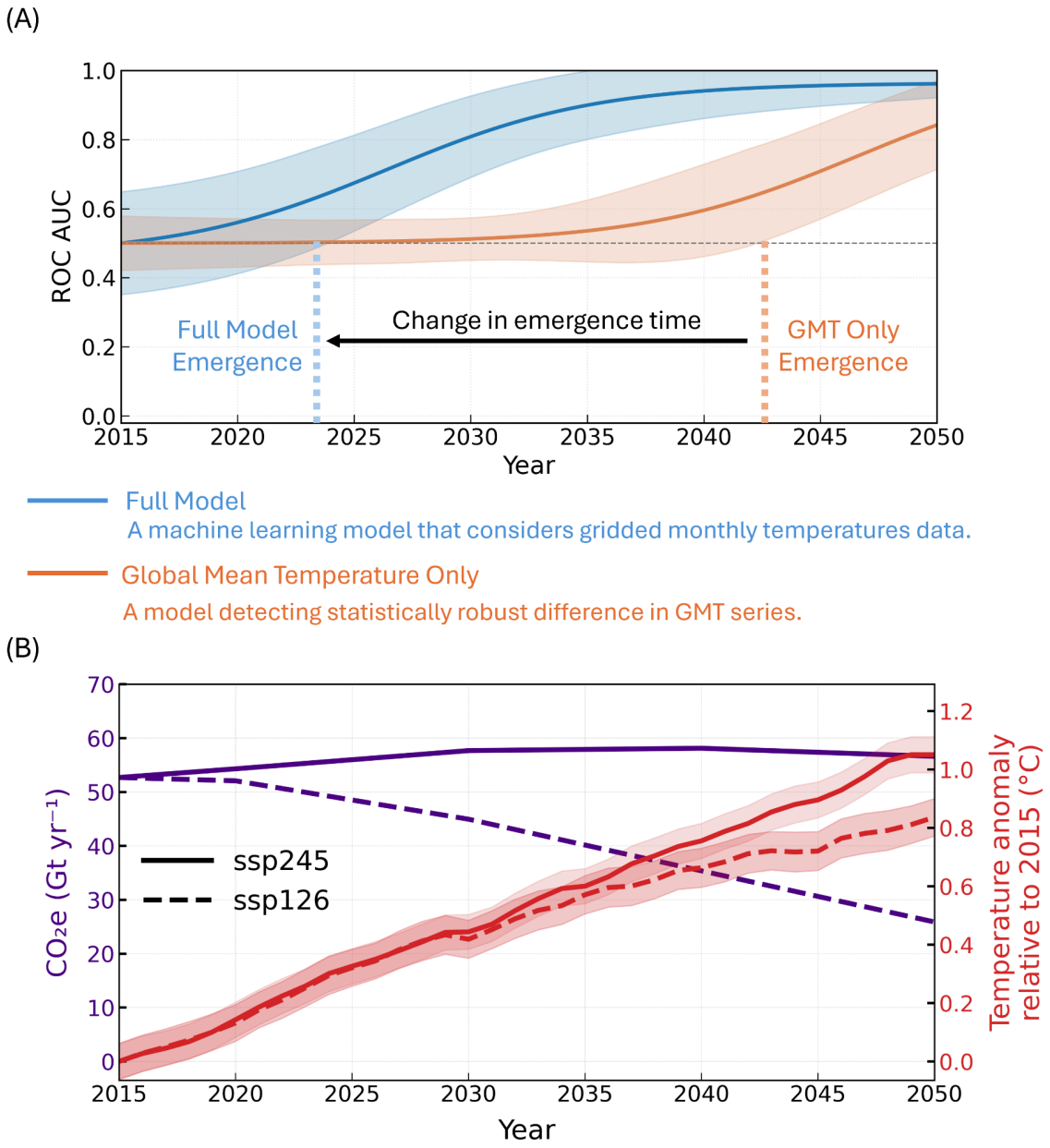

Fig. 1. Emergence times and regional drivers. *(A) Yearly ROC AUC values for the machine learning approach (blue) and the global-mean baseline model (orange). The ML model distinguishes between low- and intermediate-emissions scenarios within ≈9 years, while the baseline requires nearly 30 years for a statistically significant separation. Shaded regions represent LOESS-smoothed ±1 standard deviation across models, reflecting inter-model variability in predictive skill over time. (B) Projected annual GWP100 CO_2-equivalent (CO_2e) emissions (purple, left axis) and corresponding global mean temperature anomalies (red, right axis) for the SSP1-2.6 (dashed line) and SSP2-4.5 (solid line) scenarios, from 2015 to 2050. Temperature anomalies are calculated relative to a 2015 multi-model mean baseline. Shaded areas represent the 95% confidence interval of the temperature anomaly in the ensembles.*

Regional drivers of emerging mitigation benefits

The spatial pattern of the timing of emergence shows pronounced regional contrasts, with the Tropics standing out as the earliest emerging regions (33). Additional regions contributing strongly to early detection include North America, South and East Asia, Western Europe, and the Mediterranean, while the weakest and least meaningful features appear at high latitudes, where strong year-to-year variability delays emergence and reduces detection strength (Fig. 2). These regional differences are consistent with the expected ratio of natural variability to warming rates across latitudes, in which low variability in the Tropics favors earlier emergence and high interannual variability in high-latitude regions delays detection (Fig. S1).

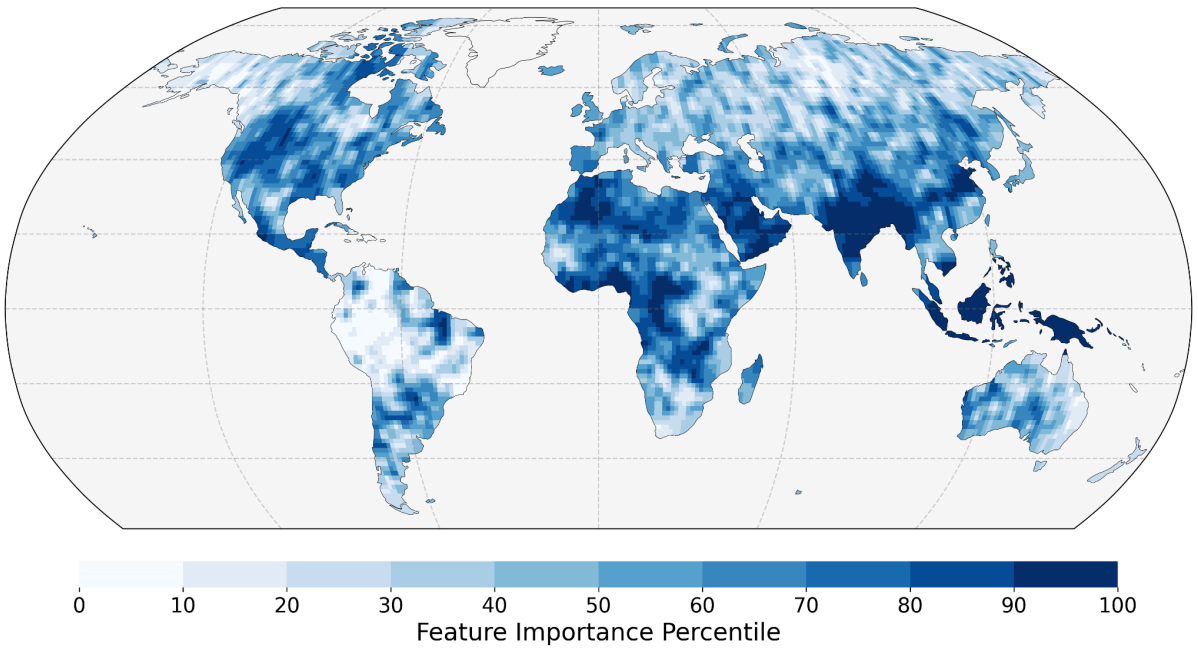

Fig. 2. Regional drivers of emergence times. *Feature importance by location, expressed as percentiles from 0 (least important) to 100 (most important), showing the relative contribution of each grid point to the model performance. Greenland and Antarctica were not included in the analysis.*

Globally, we find emergence times of 9±6 years across 30 ensemble members of five models (Table 1). The emergence times for the top four emitters and the G20 are slightly later (13 and 12 years, respectively). The slightly increased emergence time is expected given the reduced spatial information in regional subsets, yet the values remain close to the global result. To test for the sensitivity of our method to the effect of regional changes in aerosol forcing, we perform a robustness test where we

exclude South Asia, a region characterized by strong aerosol forcing and substantial reductions in near-term aerosol emissions under the mitigation scenario. We find that the resulting emergence times remain nearly unchanged, suggesting that regional aerosol variations in South Asia have limited impact on the global-scale emergence patterns.

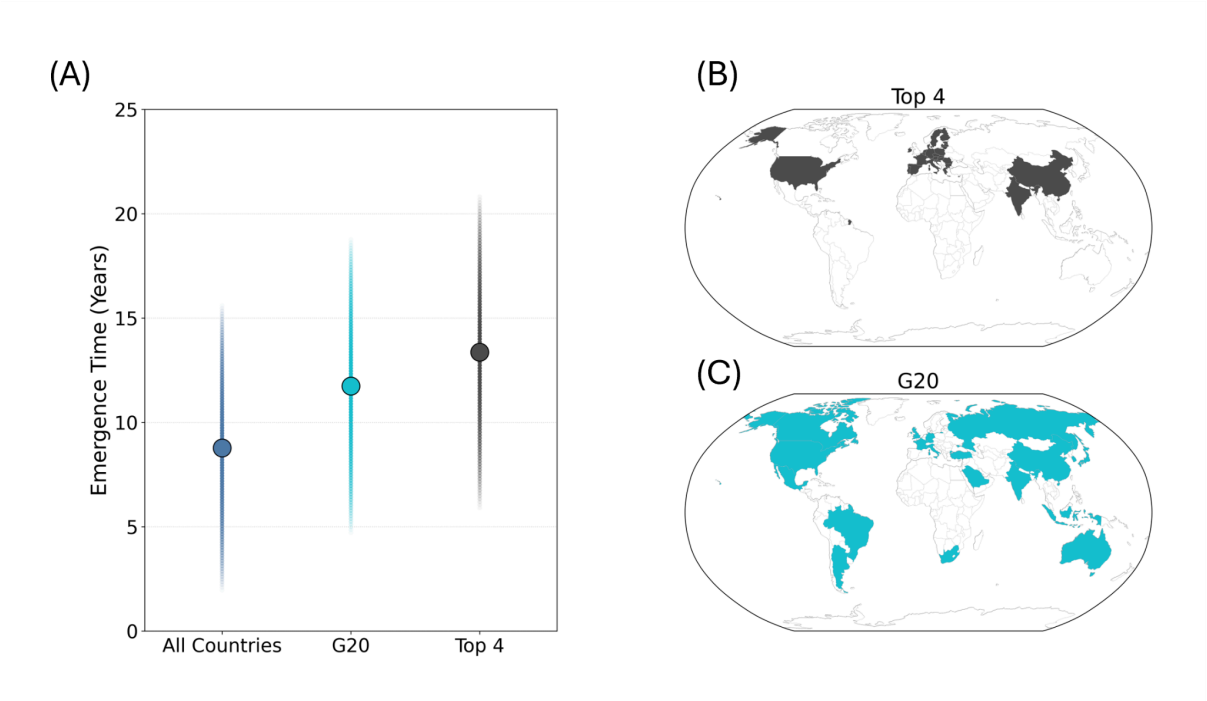

Fig. 3. Emergence time using climate data from the top four emitters subregion and the G20 subregion. *(A) Distribution of emergence times across all countries, the G20, and the top four emitters. Maps highlighting the (B) top four emitters (China, the US, India, and the EU) and (C) G20 member states. Emergence timescales are shortest for the global model (9±6 years) and slightly higher when only considering grid points within the two subgroups (13±6 years and 12±6 for the top four and G20 respectively). Group means are shown with ±1 standard deviation.*

Table 1. Emergence time by region. *Summary of emergence times between SSP1-2.6 and SSP2-4.5 for different regions. The first row shows the full global model, followed by a global dataset excluding Asia to assess the effect of aerosol changes. Subsequent rows present results for the two emission groups. The final row provides results for the global mean temperature time series, which is most comparable to previous studies. Group means are shown with ±1 standard deviation.*

Land Area	**Emergence Time (Years)**
Global*	9±6
Global* excluding South Asia	9±7
Top four emitters	13±6
G20	12±6
Global mean only	28±5

*(excluding Greenland and Antarctica)

Improved estimates of emergence time from increased model resolution

The detection skill improves with ensemble size and higher spatial resolution. The substantially earlier detection time of our full model compared with a GMT only approach suggests that spatial information, affecting the representation of local climate features, is critical. We test this hypothesis by systematically varying the spatial resolution and find a clear dependence of the emergence time (Fig. 4A). We note that the spatial resolution of our full model of 2.5° is considerably coarser than the output of some modern climate models (34), suggesting that further increases in spatial resolution could yield even earlier emergence of mitigation benefits. Similarly, we find a clear dependency of the emergence time on the number of ensemble members. Increasing the ensemble size reduces the influence of internal variability in individual simulations, enabling earlier detection of the forced signal. This effect may saturate for large ensembles (lower left corner of Fig. 4B). For Can-ESM5 and EC-Earth3, models with more than 30 members, we extend the analysis to include up to 50 members (Fig. S2). For these two models, the results do not improve beyond 30 ensemble members, although this may not hold in all cases.

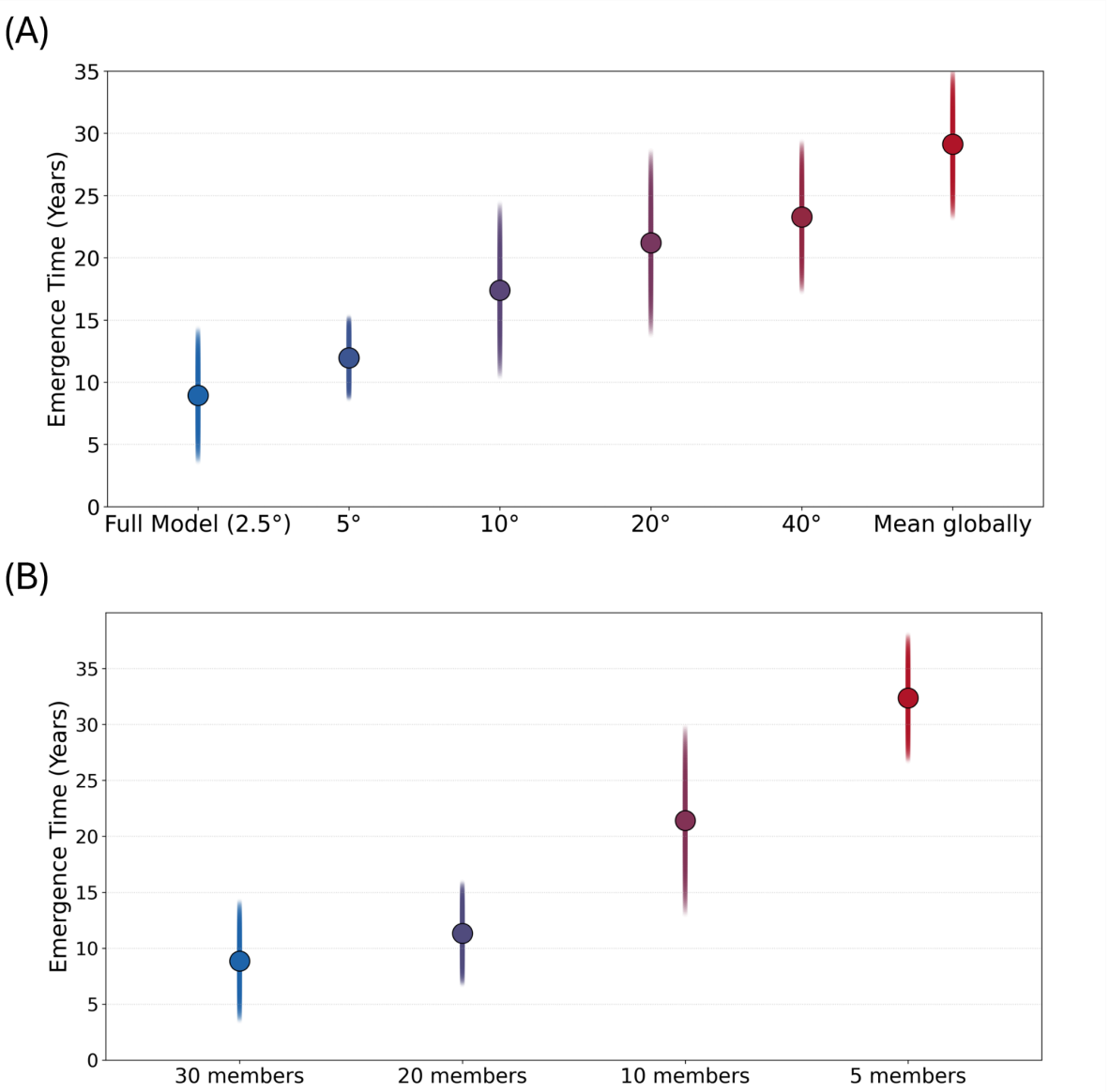

Fig. 4. Emergence time sensitivity tests. *(A) Emergence time as a function of model spatial resolution, showing the distribution from the full 2.5° grid (blue) to the global mean (red). (B) Emergence time as a function of ensemble size, starting with the full 30-member ensemble and repeating the analysis with subsets of 20, 10, and 5 members.*

Primary drivers of emergence timescales

Testing for near-term signal emergence requires comparison with a current-policy scenario, which warms at roughly 0.2 °C per decade or more over the coming

decades (Fig. S3). This raises the question of the relative importance of forcing differences vs. the timeseries length.

To explore this, as a complementary analysis, we assessed model performance as a function of the global mean temperature difference (ΔGMT) rather than calendar year (Fig. 5). For each emissions scenario, simulations were paired across baseline decades from 2020 to 2070 with future periods up to 30 years later. For each pair, we estimated ΔGMT and evaluated classification performance. Predictive skill increases primarily with ΔGMT, with clear discrimination emerging once warming exceeds ≈0.25 °C. Differences between SSP1-2.6 and SSP2-4.5 (Fig. S4) are small during the early decades; however, as the warming rate in SSP1-2.6 slows down considerably in the 2040s, SSP1-2.6 produces more pairs with small ΔGMT but large Δyears, reflecting the scenario's stabilization and even slow warming reversal after peak warming. We find that the classification performance depends primarily on ΔGMT, with ΔGMT of about 0.25°C robustly leading to detectable differences even for shorter timescales of just about five years. Yet, results for the peak-and-decline scenario SSP1-2.6 indicate that much smaller differences in GMT, of the order of 0.05-0.1°C may be detectable if timescales are sufficiently long for a discernible signal to emerge. This points to the importance of understanding the timescales of regional climate changes to the global forcing. Slowly responding equilibration processes in the climate system may continue for decades to centuries even under global temperature stabilisation (35, 36).

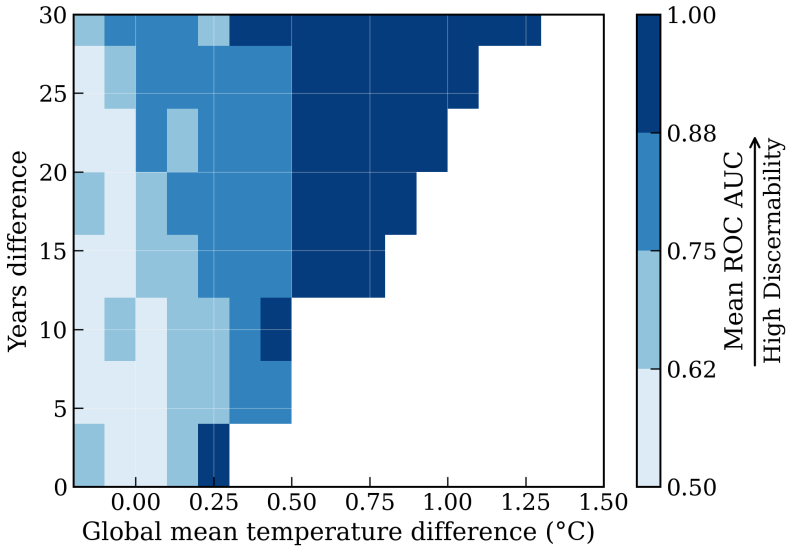

Fig. 5. Detection skill across global mean temperature difference and time separations. *Mean ROC AUC for year pairs differing by Δ years (vertical) and Δ global mean temperature (horizontal), averaged across all ensemble members starting from baseline decades between 2020 and 2070 for SSP1-2.6. White cells indicate bins with no data. Results for SSP2-4.5 and separation by model are provided in the Supplementary Information (Fig. S4).*

Discussion

Our results show that the benefits of mitigation can be detected within a decade when spatially resolved climate information is used. This differs substantially from previous estimates of 20-30 years based on traditional statistical approaches and variability of global mean temperature values (14, 16). By leveraging the full gridded output of climate models, the machine learning approach captures spatially heterogeneous signals that are masked in global averages, enabling earlier detection in regions where the forced signal rises above local variability.

The timing of emergence varies substantially across regions, as expected from physical considerations of the climate system. Feature attribution methods highlight which regions and climate variables contribute most to early emergence, linking data-driven detection to underlying physical mechanisms. We find that signals of mitigation emerge earliest in the Tropics, while early detectable signals also appear in North America, South and East Asia, Western Europe, the Mediterranean, and other regions. These differences reflect the combined influence of local warming rates and the magnitude of natural variability. Equatorial regions have low variability and moderate warming, which favours earlier emergence. Polar regions warm

rapidly but have large year-to-year variability, which delays emergence. This reinforces earlier findings on the critical role of spatial heterogeneity in detection studies (16, 37).

The early emergence of mitigation benefits has important implications. Detectable regional signals within a single decade counter the perception that mitigation yields no measurable near-term gains, a view that can weaken public and political support where planning horizons are short (38). Demonstrating that mitigation produces a discernible climate response within a decade provides a clearer scientific basis for maintaining and accelerating ambitious emissions-reduction efforts.

Several caveats remain. The analysis relies on climate model output, which may not fully capture observed variability or regional processes. Emergence times are also sensitive to the choice of scenarios, ensemble size, and statistical thresholds. Nonetheless, the sharp contrast with GMT-based estimates is robust across models and methods, indicating that early emergence is a general and detectable feature when spatial information is retained. Future work could further improve these results by using larger ensemble sizes, higher temporal resolution (i.e. daily data), or models with higher spatial resolution (Fig. 4), and by extending the analysis to additional variables including extreme event indicators, which may yield even earlier signals. We also note that our analysis focused on the SSP1-2.6 Low scenario rather than on Very Low scenarios such as SSP1-1.9, which involve substantially more stringent near-term emissions reductions toward net zero CO2 by mid-century.

Our findings underscore that climate benefits of stringent mitigation emerge in the near-term and are measurable. This is the case also for the world's highest emitters (Fig. 3), who are responsible for over 50% (Top 4) and more than 75% of global emissions (G20), respectively (39, 40), and therefore have the biggest leverage on the global emissions curve. Our results suggest that mitigation would generate detectable domestic climate benefits for these countries on near term timescales that are relevant for policy planning. This comes in addition to the wide ranging benefits of early mitigation, including improved public health due to reduced air pollution and economic gains from technology leadership (10). Our results strengthen the evidence base for urgent climate action by showing that the climate benefits of mitigation emerge rapidly and are measurable within a decade.

Methods

Data

We use monthly near-surface air temperature (minimum, mean, and maximum) from the ETH Zurich “next generation” archive of Coupled Model Intercomparison Project Phase 6 (CMIP6) simulations (30) with 2.5° × 2.5° grid data. Each training sample corresponds to one ensemble member-year and contains the full land temperature field, with minimum, mean and maximum monthly temperature stored as separate features for every grid cell. Greenland and Antarctica were excluded because their sparse observational constraints and extensive ice cover make surface air temperature trends less reliable and not directly comparable to continental regions. The raw temperature values are used directly without normalization or standardization, as tree-based models such as LightGBM do not require feature scaling.

To ensure sufficient sample size for training, we use the five models with the largest number of available records: EC-Earth3, CanESM5, MIROC6, ACCESS-ESM1-5, and MPI-ESM1-2-LR. To enable a fair comparison across models, larger ensembles were subsampled to 30 members. We treat SSP1-2.6 as the low-emissions scenario and SSP2-4.5 as the intermediate-emissions scenario.

Methodology

For each climate model, we first obtain the available ensemble members for the selected low- and intermediate-emissions scenarios. We then apply a leave-one-out approach (41): for each ensemble member, we train the model using all other members and use the held-out member as the test set. This procedure is repeated for every year from 2015 to 2050, with the training data including all observations from 2015 up to the target year. We cap the training window at the five most recent years once available, as these years are expected to be the most informative for distinguishing the evolving temperature response under different scenarios. A leave-one-out design prevents leakage across ensemble members, with the held-out member used only for testing, and future years are excluded from training, ensuring that the model never accesses information from either the test member or later years.

In each iteration, we train a LightGBM (29, 42) classifier on the training data to distinguish between the low- and intermediate-emissions scenarios. LightGBM is a gradient-boosted decision tree algorithm well suited for high-dimensional tabular data (29, 42) with consistently strong performance in classification tasks (32). The LightGBM classifier is trained with 200 estimators, learning rate of 0.05, 64 leaves per tree with no maximum depth, subsampling of 0.8 for both rows and columns, and L2 regularization. A separate LightGBM model is trained for each year. The probability estimates from these yearly models are then provided to a logistic regression meta-model, which predicts the overall probability. The meta-model's prediction probabilities are evaluated on the held-out test member, with the ROC AUC (area under the receiver operating characteristic curve) used as the performance metric (31). The ROC AUC quantifies how well the model ranks positive cases above negative ones across all classification thresholds, with a value of 0.5 indicating no discriminative ability (random guessing) and 1 indicating perfect separation between the scenarios.

The procedure yields a ROC AUC score for each year. In the first years after 2015, the score is expected to be low, as the low- and intermediate-emissions scenarios remain similar. Over time, the scenarios diverge, and the ROC AUC is expected to increase, eventually approaching 1. We fit a sigmoid function to the ROC AUC values as a function of year. The emergence year is defined as the first year in which the confidence interval of the fitted curve, given by the LOESS-smoothed (43) standard deviation across models (mean ± 1 standard deviation), exceeds the random-guess threshold of 0.5. Fig. S5 presents an overview of the research workflow.

One potential concern is that the signal may reflect changes in aerosols rather than long-term temperature trends. To address this, we also repeat the analysis for the entire global land area excluding South Asia, where aerosol changes between scenarios are particularly pronounced (44).

To interpret the model's behavior, we conduct an explainability analysis by examining the relative importance of each spatial region in the LightGBM models (24), presented in Fig. 2. Feature importance values are averaged across ensemble members to identify the regions that most strongly drive scenario discrimination,

revealing where the earliest and most robust signals of scenario divergence emerge. As a complementary analysis, we also repeat the model experiments using data restricted to selected regions, focusing on the top four emitting countries and the G20 nations (Fig. 3).

As a performance baseline, we repeat the process without the gridded data or machine learning models. Instead, we use only the global mean surface air temperature as input to a logistic regression model and evaluate its performance over time. As expected, this approach yields relatively long emergence timescales of about 30 years, consistent with previous studies (14, 16).

To assess the robustness of the results, we also evaluate how spatial resolution and ensemble size affect the estimated emergence times (Fig. 4). Model experiments are repeated at multiple spatial resolutions, from 2.5° grids to global means, and with varying ensemble sizes, starting from the full dataset of 30 members per model and decreasing to 5. These tests quantify how spatial aggregation and ensemble size influence the detectability of scenario differences and the timing of emergence.

As a complementary analysis, we evaluate model performance as a function of the global mean temperature difference (ΔGMT) rather than calendar year (Fig. 5). For each emissions scenario separately (e.g., SSP2-4.5), we form pairs of years within the same scenario, consisting of a baseline year and a future year. We repeat this procedure for successive baseline decades from 2020 to 2070, pairing each baseline period with future years up to 30 years later. For each pair, we compute ΔGMT and evaluate the model's ability to distinguish the two time periods. This analysis isolates how predictive skill depends on ΔGMT rather than on the choice of model, showing how the classification performance depends on global temperature difference and time difference.

Data availability

All climate model simulations used in this study are available through The ETH Zurich CMIP6 next generation archive (30) (https://zenodo.org/records/3734128).

Code availability

The analysis code used in this study is provided as part of the submission. Upon acceptance, the code will be deposited in Zenodo with a permanent DOI and the link will be added to this section. No proprietary software was used.

Acknowledgements

We thank Gidon Eshel and Annika Högner for their insights and intellectual support for this study. We thank The ETH Zurich CMIP6 next generation archive for making their data available. A.S. acknowledges support from the Council for Higher Education Energy and Climate Postdoctoral Fellowship. R.M. is Head of the Institute for Environmental Sustainability and an incumbent of the Charles and Louise Gartner Professorial Chair.

Funding

None to declare.

Supporting Information

Fig. S1 shows emergence times derived from a baseline analysis, where at each grid cell the local temperature standard deviation is divided by the difference in warming rates between the low- and intermediate-emission scenarios. In this approach, faster warming and lower natural variability yield shorter emergence timescales. The figure highlights regions where shorter timescales are expected.

Notably, equatorial regions, particularly the maritime continent, exhibit shorter emergence timescales due to the low natural variability of their climate. In these regions, even relatively small temperature changes are pronounced because of the stable baseline. In contrast, regions with high warming rates, such as the Arctic, show longer emergence timescales because their natural climate variability is especially large.

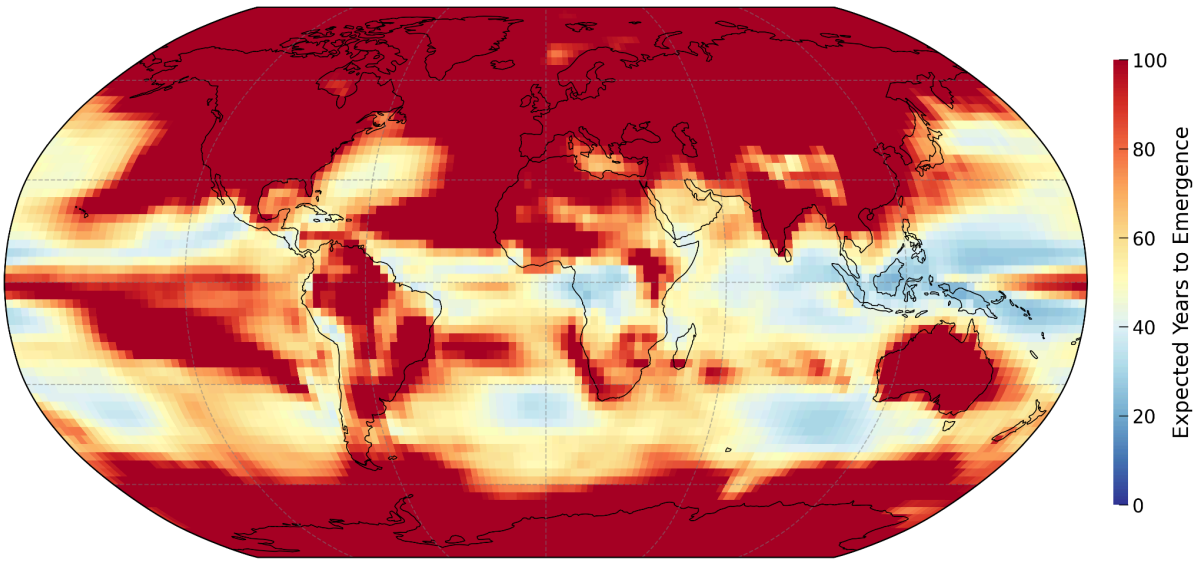

Fig. S1. Expected emergence time by a naive algorithm. *The estimate is obtained by dividing the standard deviation of temperature by the difference in annual warming rates between the SSP2-4.5 and SSP1-2.6 scenarios, for each region. The shortest emergence times appear in the Tropics, primarily due to their low temperature variability.*

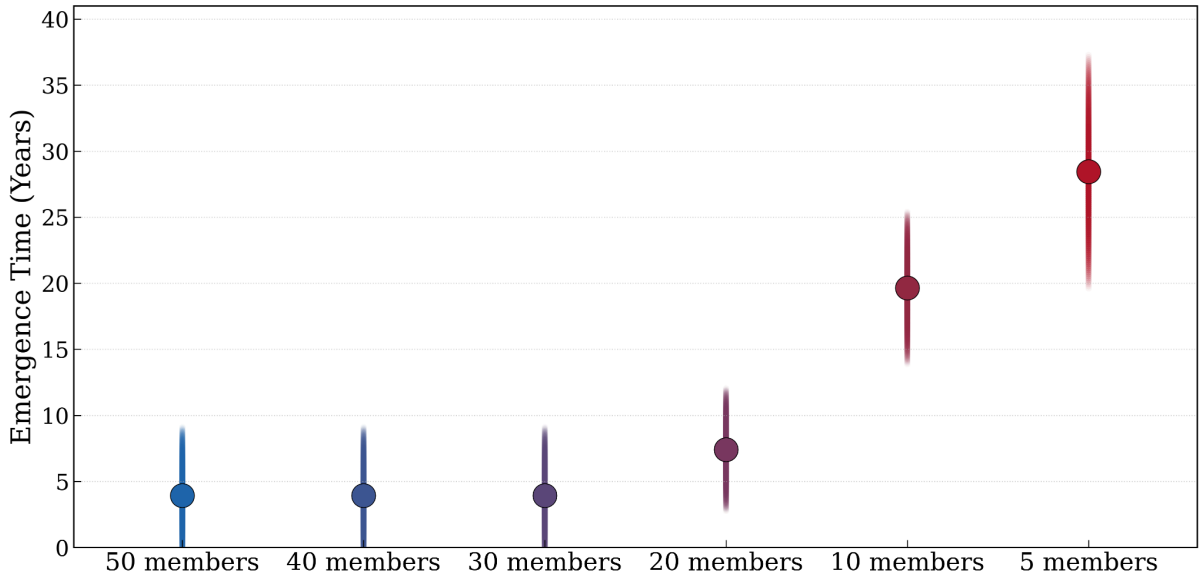

Fig. S2. Emergence time sensitivity to ensemble size. *As in Fig. 4B, emergence time is evaluated from varying ensemble sizes, using up to 50 members and repeating the analysis with subsets of 40, 30, 20, 10, and 5 members. Because only CanESM5 and EC-Earth3 provide 50 ensemble members, results are restricted to those two models.*

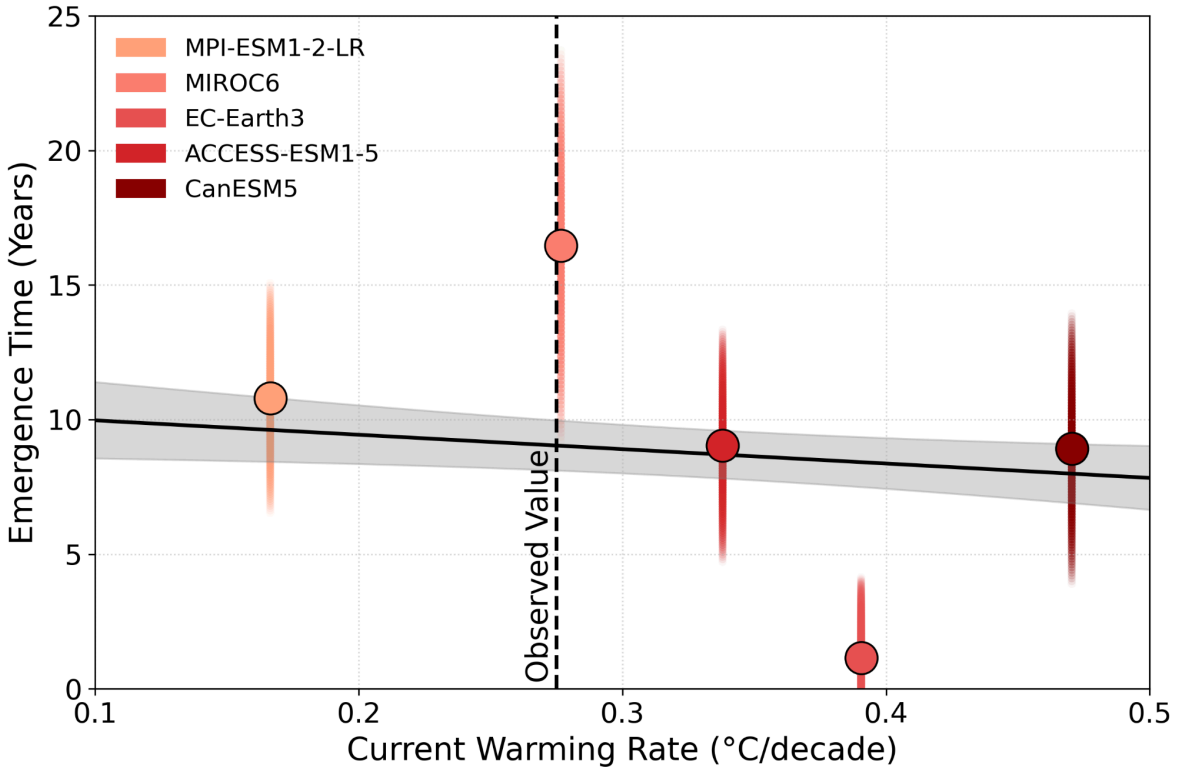

Fig. S3. Emergence times by model. *Emergence times based on the full gridded Earth for each examined model. On average, higher warming rates result in shorter emergence times. The vertical line indicates the observed global temperature trend for 2015–2024 (45) .*

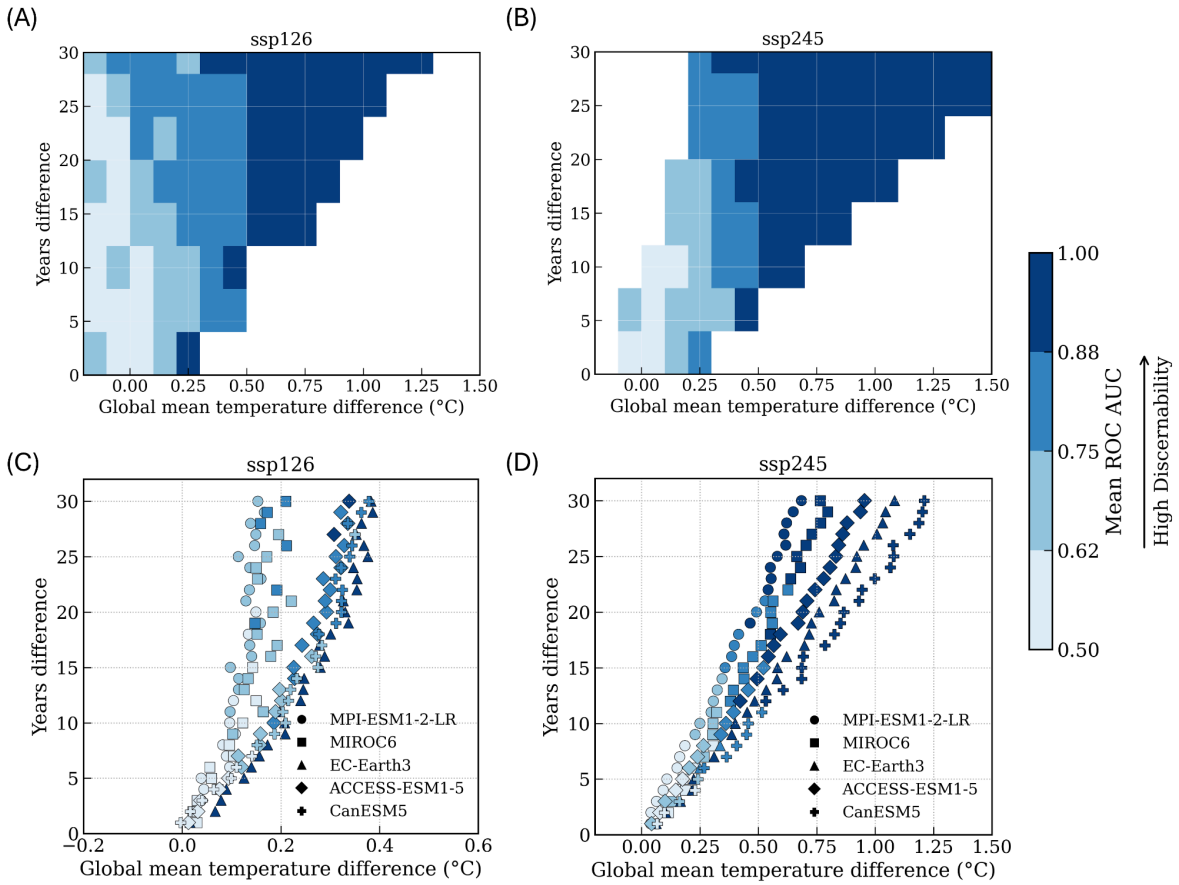

Fig. S4. Detection skill across Δ Global Mean Temperature and time separations. *Panels (A–B) show mean ROC AUC for year pairs differing by Δ years (vertical) and Δ global mean temperature (horizontal), averaged across all simulations starting from baseline decades between 2020 and 2070. White cells indicate bins with no data. Panels (C–D) show results for individual models, where each point represents a pair of decades separated by up to 30 years. Darker colors indicate higher classification skill (ROC AUC).*

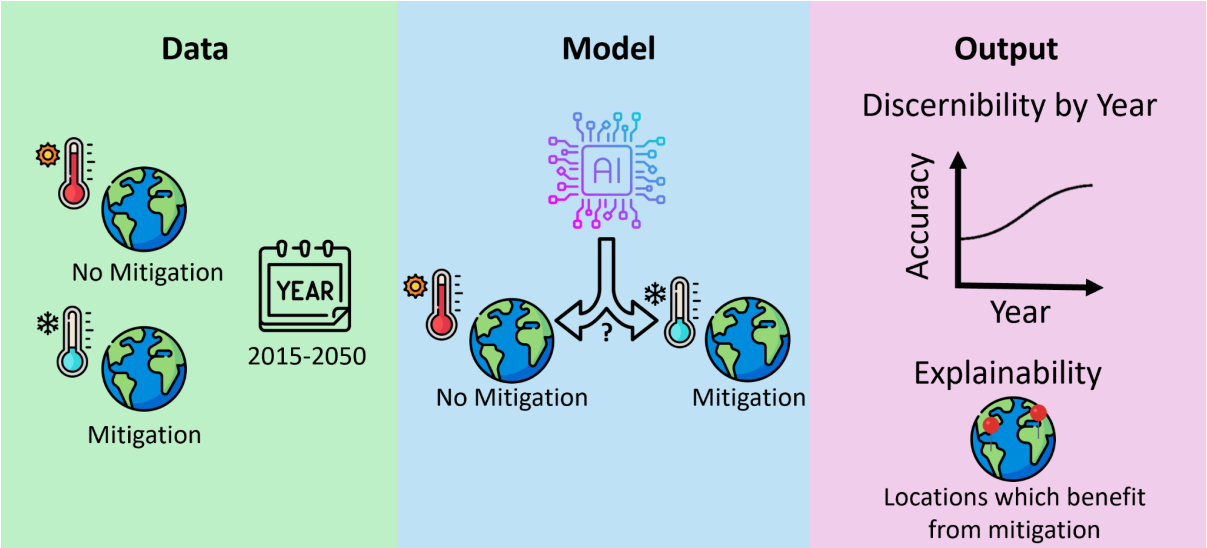

Fig. S5. Schematic overview of the study framework. *Climate simulations are collected for mitigation and no-mitigation scenarios, namely SSP1-2.6 and SSP2-4.5, covering the period 2015-2050. These data are used to train a machine learning model designed to distinguish between the two scenarios for each individual year. The outputs include the model's discriminability over time, expressed as predictive performance by year, and an explainability analysis highlighting the regions that contribute most strongly to the model's predictive skill.*

References

1. L. Grant, *et al.*, Global emergence of unprecedented lifetime exposure to climate extremes. *Nature* **641**, 374–379 (2025).

2. G. Hansen, D. Stone, Assessing the observed impact of anthropogenic climate change. *Nat. Clim. Chang.* **6**, 532–537 (2016).

3. A. Robinson, J. Lehmann, D. Barriopedro, S. Rahmstorf, D. Coumou, Increasing heat and rainfall extremes now far outside the historical climate. *Npj Clim. Atmos. Sci.* **4** (2021).

4. K. E. Trenberth, J. T. Fasullo, T. G. Shepherd, Attribution of climate extreme events. *Nat. Clim. Chang.* **5**, 725–730 (2015).

5. K. E. Trenberth, *et al.*, Global warming and changes in drought. *Nat. Clim. Chang.* **4**, 17–22 (2014).

6. P. Stott, How climate change affects extreme weather events. *Science* **352**, 1517–1518 (2016).

7. J. J. Hellmann, J. E. Byers, B. G. Bierwagen, J. S. Dukes, Five potential consequences of climate change for invasive species. *Conserv. Biol.* **22**, 534–543 (2008).

8. J.-C. Ciscar, *et al.*, Physical and economic consequences of climate change in Europe.

Proc. Natl. Acad. Sci. U. S. A. **108**, 2678–2683 (2011).

9. C. Schleussner, *et al.*, Differential climate impacts for policy-relevant limits to global warming: the case of 1.5 °C and 2 °C. *Earth System Dynamics Discussions* **7**, 327–351 (2015).

10. P. R. S. J. S. R. S. A. A. K. R. van Diemen D. McCollum M. Pathak S. Some P. Vyas R. Fradera M. Belkacemi A. Hasija G. Lisboa S. Luz J. Malley (eds.), *IPCC, 2022: Summary for Policymakers. In: Climate Change 2022: Mitigation of Climate Change. Contribution of Working Group III to the Sixth Assessment Report of the Intergovernmental Panel on Climate Change* (Cambridge University Press, Cambridge, UK and New York, NY, USA. doi: 10.1017/9781009157926.001).

11. A. Lanson, P. Pfleiderer, F. Lehner, C. Schleussner, Uncertainty in near-term temperature evolution must not obscure assessments of climate mitigation benefits. *Nat. Commun.* **13** (2020).

12. K. E. Tiede, H. Temme, L. Lehrer, C. Betsch, Enhancing perceived effectiveness can increase climate policy acceptance. *J. Environ. Psychol.* **106**, 102725 (2025).

13. *IPCC, 2021: Summary for Policymakers. In: Climate Change 2021: The Physical Science Basis. Contribution of Working Group I to the Sixth Assessment Report of the Intergovernmental Panel on Climate Change* (Cambridge University Press, Cambridge, United Kingdom and New York, NY, USA, pp. 3−32, doi:10.1017/9781009157896.001).

14. C. Tebaldi, P. Friedlingstein, Delayed detection of climate mitigation benefits due to climate inertia and variability. *Proc. Natl. Acad. Sci. U. S. A.* **110**, 17229–17234 (2013).

15. B. Samset, J. Fuglestvedt, M. Lund, Delayed emergence of a global temperature response after emission mitigation. *Nat. Commun.* **11** (2020).

16. N. Maher, F. Lehner, J. Marotzke, Quantifying the role of internal variability in the temperature we expect to observe in the coming decades. *Environ. Res. Lett.* **15**, 054014 (2020).

17. K. L. Ricke, K. Caldeira, Maximum warming occurs about one decade after a carbon dioxide emission. *Environ. Res. Lett.* **9**, 124002 (2014).

18. C. M. McKenna, A. C. Maycock, P. M. Forster, C. J. Smith, K. B. Tokarska, Stringent mitigation substantially reduces risk of unprecedented near-term warming rates. *Nat. Clim. Chang.* **11**, 126–131 (2021).

19. Intergovernmental Panel on Climate Change (IPCC)., *Linking Global to Regional Climate Change. In Climate Change 2021 – The Physical Science Basis: Working Group I Contribution to the Sixth Assessment Report of the Intergovernmental Panel on Climate Change (pp. 1363–1512). chapter 10, Cambridge: Cambridge University Press* (2023).

20. D. Bzdok, M. Krzywinski, N. Altman, Points of Significance: Machine learning: a primer. *Nat. Methods* **14**, 1119–1120 (2017).

21. S. Rasp, M. S. Pritchard, P. Gentine, Deep learning to represent subgrid processes in climate models. *Proc. Natl. Acad. Sci. U. S. A.* **115**, 9684–9689 (2018).

22. M. Reichstein, *et al.*, Deep learning and process understanding for data-driven Earth system science. *Nature* **566**, 195–204 (2019).

23. I. Price, *et al.*, Probabilistic weather forecasting with machine learning. *Nature* **637**, 84–90 (2025).

24. J. S. Dramsch, *et al.*, Explainability can foster trust in artificial intelligence in geoscience. *Nat. Geosci.* **18**, 112–114 (2025).

25. A. Bracco, *et al.*, Machine Learning for the physics of climate. *arXiv [physics.ao-ph]* (2024).

26. G. Camps-Valls, *et al.*, Artificial intelligence for modeling and understanding extreme weather and climate events. *Nat. Commun.* **16**, 1919 (2025).

27. V. Eyring, *et al.*, Pushing the frontiers in climate modelling and analysis with machine learning. *Nat. Clim. Chang.* **14**, 916–928 (2024).

28. N. Burkart, M. F. Huber, A survey on the explainability of Supervised Machine Learning. *J. Artif. Intell. Res.* **abs/2011.07876** (2020).

29. G. Ke, *et al.*, LightGBM: A highly efficient Gradient Boosting Decision Tree. *Neural Inf Process Syst* 3146–3154 (2017).

30. L. Brunner, M. Hauser, R. Lorenz, U. Beyerle, The ETH Zurich CMIP6 next generation archive: technical documentation. *ETH Zürich, Zürich, 2020* [Preprint] (2020). Available at: http://dx.doi.org/10.5281/ZENODO.3734128.

31. A. P. Bradley, The use of the area under the ROC curve in the evaluation of machine learning algorithms. *Pattern Recognit.* **30**, 1145–1159 (1997).

32. A. Shmuel, O. Glickman, T. Lazebnik, A comprehensive benchmark of machine and deep learning models on structured data for regression and classification. *Neurocomputing* **655**, 131337 (2025).

33. C. Mora, *et al.*, The projected timing of climate departure from recent variability. *Nature* **502**, 183–187 (2013).

34. R. J. Haarsma, *et al.*, High Resolution Model Intercomparison Project (HighResMIP v1.0) for CMIP6. *Geosci. Model Dev.* **9**, 4185–4208 (2016).

35. A. D. King, *et al.*, Exploring climate stabilisation at different global warming levels in ACCESS-ESM-1.5. *Earth Syst. Dyn.* **15**, 1353–1383 (2024).

36. F. Lacroix, F. A. Burger, Y. Silvy, C.-F. Schleussner, T. L. Frölicher, Persistently elevated high‐latitude ocean temperatures and global sea level following temporary temperature overshoots. *Earths Future* **12** (2024).

37. Y.-R. Wang, D. O. Hessen, B. H. Samset, F. Stordal, Evaluating global and regional land warming trends in the past decades with both MODIS and ERA5-Land land surface temperature data. *Remote Sens. Environ.* **280**, 113181 (2022).

38. A. Alesina, G. Tabellini, Bureaucrats or politicians? Part II: Multiple policy tasks. *J. Public Econ.* **92**, 426–447 (2008).

39. M. Banja, *et al.*, A comparative analysis of EDGAR and UNFCCC GHG emissions 1 inventories: insights on trends, methodology and data discrepancies. *Earth System , 2025*.

40. R. Garaffa, *et al.*, Stocktake of G20 countries' climate pledges reveals limited

macroeconomic costs and employment shifts. *One Earth* **6**, 1591–1604 (2023).

41. T.-T. Wong, Performance evaluation of classification algorithms by k-fold and leave-one-out cross validation. *Pattern Recognit.* **48**, 2839–2846 (2015).

42. D. Zhang, Y. Gong, The comparison of LightGBM and XGBoost coupling Factor Analysis and prediagnosis of Acute Liver Failure. *IEEE Access* **8**, 220990–221003 (2020).

43. W. S. Cleveland, S. J. Devlin, Locally weighted regression: An approach to regression analysis by local fitting. *J. Am. Stat. Assoc.* **83**, 596–610 (1988).

44. M. T. Lund, G. Myhre, B. H. Samset, Anthropogenic aerosol forcing under the Shared Socioeconomic Pathways. *Atmospheric Chemistry and Physics* **19**, 13827–13839 (2019).

45. P. Forster, *et al.*, Indicators of Global Climate Change 2024: annual update of key indicators of the state of the climate system and human influence. *Earth Syst. Sci. Data* (2025). https://doi.org/10.5194/essd-17-2641-2025.